Journal of Materials Chemistry C

ROYAL SOCIETY OF CHEMISTRY

PAPER

View Article Online
View Journal | View Issue

Cite this: J. Mater. Chem. C, 2025, 13, 4413

A study on device physics of deep ultraviolet light emitting diodes leveraging machine learning†

Na Lin,[a] Zhiqiang Liu,[b] Zhuoying Jiang,[a] Ying Jiang,[a] Shanshan Zhao,[a] Jinjian Yan,[b] Sijie Jiang,[a] Yikai Yun,[a] Wenjie Wei,[a] Shaoqun Li,[a] Ziang Wan,[a] Jianfeng Du,[a] Jinchai Li,[bcd] Tao Tao,[e] Kai Huang,*[bcd] Lin Li,*[a] Mengyu Chen,*[ad] Cheng Li*[ad] and Rong Zhang[bcde]

Received 13th November 2024,
Accepted 16th January 2025

DOI: 10.1039/d4tc04816d

rsc.li/materials-c

Aluminum gallium nitride (AlGaN)-based deep ultraviolet (DUV) light-emitting diodes (LEDs) hold tremendous potential and application prospects. However, DUV LEDs face challenges such as low internal quantum efficiency (IQE) and degraded luminous performance because of properties intrinsic to aluminum-rich group III-nitride materials. To address these challenges, traditional trial-and-error experimental methods are commonly employed. However, with rapid industrial advancements, this approach has become inadequate to meet current demands. In this work, this study demonstrates an effective approach to optimize the luminous performance of DUV LEDs using machine learning (ML). By training 4 typical ML models with a dataset of AlGaN-based LED structures compiled over the past decade and more, we find that the convolutional neural network (CNN) provides the most accurate predictions, with a root mean square error (RMSE) of 1.6995 W cm^{-2} and a coefficient of determination (R^2) of 0.9812 for the light output power density (LOPD). Using the CNN model, we reveal the key features that influence the luminous performance of DUV LEDs. In addition, we explore the relationships between different features and LOPD, which align with physical mechanisms and are generally consistent with simulation and experimental results. Overall, this work demonstrates that ML is capable of predicting device performance, extracting critical features from complex structures, and significantly aiding in the optimization of DUV LEDs.

Introduction

Deep ultraviolet (DUV) light plays a crucial role in various fields, including medical treatments,[1] disinfection,[2] communication,[3] and growth lighting.[4] Traditionally, ultraviolet (UV) light sources rely on mercury lamps, which present several drawbacks, such as bulkiness, limited lifespan, toxicity, and prolonged warm-up times. In contrast, III-nitride-based UV light-emitting diodes (LEDs) have gained attention as a superior alternative, offering higher energy efficiency, environmental sustainability, and enhanced performance.[5] Aluminum gallium nitride (AlGaN) as a direct-band-gap material can tune in the range of 3.4–6.2 eV by changing the aluminum (Al) content, covering the whole UV wavelength range from 200 to 365 nm, making it the preferred material for fabricating DUV LEDs.[6]

While UVA-LEDs with emission wavelengths above 315 nm exhibit external quantum efficiencies (EQEs) exceeding 50%, LEDs in the UVB and UVC band lag significantly behind. Although recent reports indicated peak EQEs of up to 20% for DUV LEDs near 275 nm,[7] commercial devices in these wavelength ranges still achieve performance in the single-digit percentage range.[8] This reduced EQEs can be attributed to three primary factors: low light extraction efficiency,[9] low carrier injection efficiency,[10] and polarization field-induced reduction in radiative recombination efficiency.[11] Consequently, improving the EQEs of DUV LEDs remains a major focus in current UV LEDs research, particularly in the domain of LEDs design optimization. Zhang *et al.* had proposed a p-type electron blocking layer (EBL) with the graded AlN composition, which significantly boosted the EQEs and light output power density (LOPD) of DUV LEDs by 1.5 times.[12] Hu *et al.* improved radiative recombination by designing a superlattice electron deceleration layer to slow down electrons injected into the active region.[13] Nevertheless, the complex

[a] School of Electronic Science and Engineering, Xiamen University, Xiamen 361005, P. R. China. E-mail: lilin@xmu.edu.cn, mychen@xmu.edu.cn, chengli@xmu.edu.cn
[b] Fujian Key Laboratory of Semiconductor Materials and Applications, CI Center for OSED, Department of Physics, Xiamen University, Xiamen 361005, P. R. China. E-mail: k_huang@xmu.edu.cn
[c] Engineering Research Center of Micro-nano Optoelectronic Materials and Devices, Ministry of Education, Xiamen University, Fujian, Xiamen 361005, P. R. China
[d] Future Display Institute of Xiamen, Fujian, Xiamen 361005, P. R. China
[e] Jiangsu Provincial Key Laboratory of Advanced Photonic and Electronic Materials, School of Electronic Science and Engineering, Nanjing University, Nanjing 210093, P. R. China

† Electronic supplementary information (ESI) available. See DOI: https://doi.org/10.1039/d4tc04816d

interplay of structural and compositional parameters in LEDs still makes optimizing device performance extremely challenging. Traditional optimization processes demand extensive multi-layered empirical knowledge, which is both time-consuming and costly. In this aspect, machine learning (ML)-based research methods offer potential to address these challenges and accelerate the development of AlGaN-based DUV LEDs.

ML has been widely applied in material characterization,[14] material analysis,[15] and material design[16] due to its advantages of short development cycle, low computational cost, strong data processing capabilities, and high predictive accuracy. For III-nitride-based LEDs, which have complex material compositions and intricate device structures, ML holds promise for capturing intrinsic relationships between various features and predicting device performance using extensive databases. For instance, Jiang *et al.* conducted a feature importance analysis to identify key factors affecting the performance of blue GaN-based LEDs, demonstrating that convolutional neural network (CNN) provided the most accurate predictions.[17] In the field of AlGaN-based DUV LEDs, Lin *et al.* utilized extreme gradient boosting (XGBoost) and light gradient boosting machine (LightGBM) to develop a stacked ML model aimed at predicting high-performance superlattice EBL, taking into account different compositions, thicknesses, and band offset ratios.[18] Nevertheless, this work is limited to specific layers of the device and lacks sufficient features to provide adequate prediction accuracy. This suggests that an appropriate modeling approach tailored to AlGaN-based DUV LEDs should be employed during feature selection.

In this work, we propose a ML-assisted framework to explore the key features affecting the luminous performance of AlGaN-based DUV LEDs and the relationships between these features and LEDs performance. First, we establish a dataset that includes the features describing the luminous performance of AlGaN-based DUV LEDs, including (1) structural characteristic parameters and (2) electrical characteristic parameters. Detailed description of these feature are list in the following part. The simulation data are sourced from published literature over the past 17 years, focusing on wavelengths below 310 nm. Four typical ML models, including random forest (RF),[19] XGBoost,[20] feedforward neural network (FNN),[21] and CNN[22] are trained to predict the LOPD. For interpretability analysis of the CNN model, we apply Shapley Additive exPlanations (SHAP),[23] allowing us to connect the predicted performance to the physical principles governing AlGaN-based DUV LEDs. Finally, we use the trained CNN model to predict the luminous performance of approximately 3500 LEDs devices within seconds. The reliability of the model is verified using simulation results from advanced physical models of semiconductor devices (APSYS) software as well as experimental results from previously published studies that are not included in the training set.

Results and discussion

Construction of dataset

In this work, AlGaN-based DUV LEDs grown on a *c*-plane sapphire substrate serve as a representative device for discussion. The entire working framework is illustrated in Fig. 1(a). First, a dataset is constructed to describe the characteristics of the DUV LEDs, including (1) structural characteristic parameters and (2) electrical characteristic parameters. The structural characteristic parameters encompass the thickness of various layers in the DUV LEDs, the number of cycles, composition, and doping concentration. While electrical characteristic

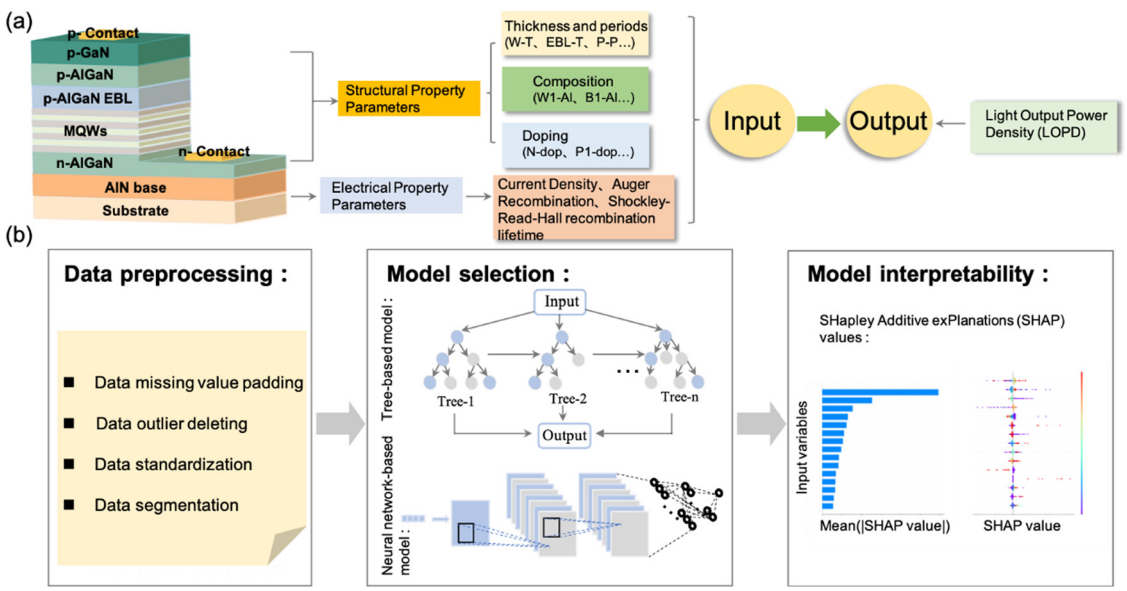

Fig. 1 The whole working framework based on ML. (a) A sketch map of the input features. The structural characteristic parameters and electrical characteristic parameters of the AlGaN-based DUV LEDs are selected as features of each sample. (b) The whole process consists of three main parts: (1) data preprocessing, (2) model selection, (3) model interpretability.

parameters pertain to the APSYS software, including the Auger recombination coefficient (Auger), Shockley–Read–Hall recombination lifetime (SRH lifetime), and current density. During feature selection, we aim to accurately and comprehensively describe the complete structure of the devices in our dataset, considering the complex structures employed in AlGaN DUV LEDs as reported in various literature. For example, features such as E1-Al (average aluminum content in the first piece of the electron blocking layer), E2-Al (average aluminum content in the second piece of the electron blocking layer), and E3-Al (average aluminum content in the third piece of the electron blocking layer) are included. A more detailed description of all 45 features are provided in Table S1 (ESI†).

As an indicator of the luminescence performance of LEDs epitaxial structures, LOPD is chosen as the target output of the ML model. The dataset consists of 378 effective samples for predicting LOPD, constructed by recording the luminance properties of LEDs structures reported in peer-reviewed journals over the past 17 years. It adheres to the following criteria: (1) the paper is published in a peer-reviewed journal; (2) the research focuses on DUV LEDs with a peak wavelength below 310 nm; (3) the paper provides LOPD values in the characterization section; and (4) the study offers a detailed description of the device structure.

Machine learning analysis

As shown in Fig. 1(b), during the data preprocessing stage, methods such as data missing value padding, data outlier deleting, data standardization, and data segmentation are employed. Briefly, the entire dataset is divided into training, validation, and testing set in a ratio of 8 : 1 : 1. The training set is used to train the model, the validation set is utilized to adjust the model's hyperparameters and evaluate its performance, and the testing set is reserved for the final evaluation of the model's generalization ability. Then, ML methods are applied for prediction, including RF, XGBoost, FNN, and CNN. Key features affecting LOPD are further analyzed using the SHAP method to enhance model interpretability. The optimized model is then employed to conduct high-throughput predictions on a conventional device structure within seconds. Subsequently, simulation results used for APSYS software and experimental results are employed to evaluate the validation of our model.

Comparison of model performance

The scatter plots of the predicted values *versus* reported values of the LOPD during the training and testing stages for four ML models are shown in Fig. 2. We employ the RMSE and the R^2 as

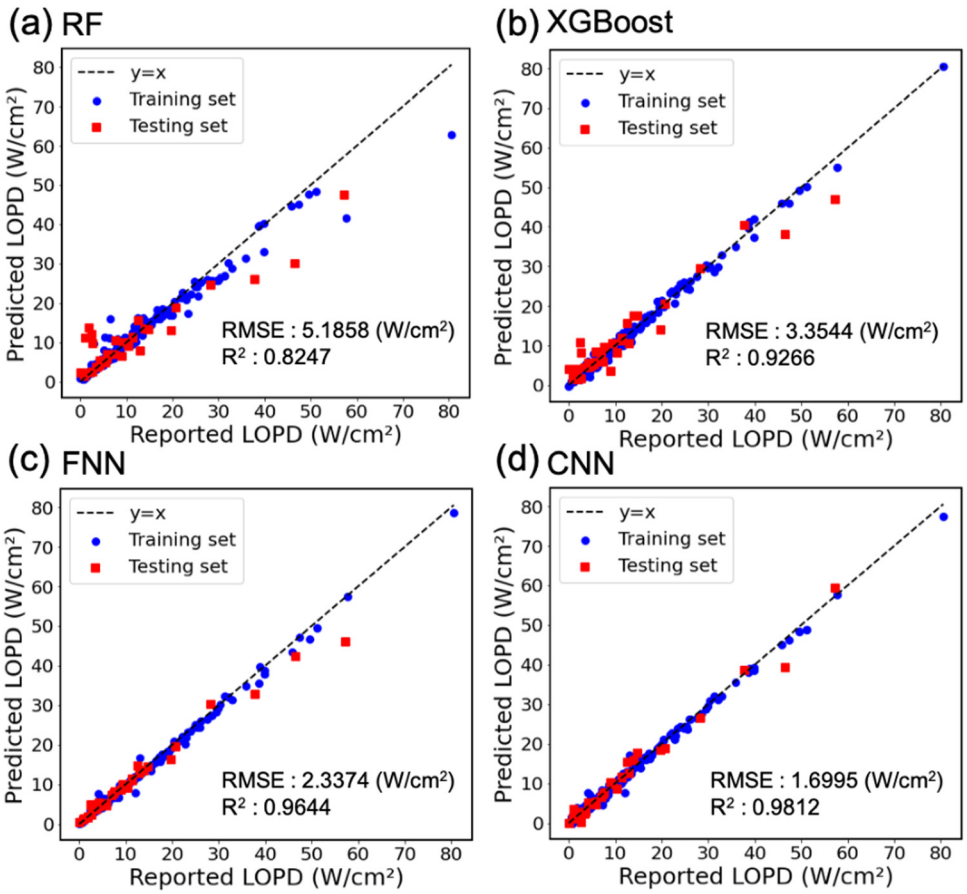

Fig. 2 The prediction performances of different models on LOPD. (a) The performance of RF model on LOPD. (b) The performance of XGBoost model on LOPD. (c) The performance of FNN model on LOPD. (d) The performance of CNN model on LOPD.

metrics to evaluate the performance of the ML model. RMSE is used to measure the deviation between predicted values and true values, while R^2 ranges between 0 and 1, with a value closer to 1 indicating better regression fitting performance. From the Fig. 2, it can be observed that the neural network-based model outperforms the tree-based model, particularly with CNN exhibiting lower RMSE at 1.6995 W cm^{-2} and higher R^2, reaching 0.9812. Compared to neural network models, tree-based models are more prone to overfitting on our dataset, making them potentially less suitable for this application. We attribute the outstanding performance of CNN to two main factors. Firstly, our feature descriptors encompass parameters related to the LEDs device structure, such as composition, doping concentration, thickness, which inherently exhibit strong interdependencies.[17] By structuring the data into a two-dimensional format, the ability of CNN to capture and learn these interactions more effectively is leveraged. Specifically, the original one-dimensional feature array is reshaped into a 5×9 matrix. The arrangement of the features is based on their physical relevance and potential interactions. For instance, features related to the thickness, doping concentration and composition of each layer are tightly connected according to their physical relevance, reflecting their interrelated impact on the overall LEDs performance. Consequently, by leveraging convolutional kernels, CNN can effectively learn the coupling relationships between features. Secondly, neural network, due to their hierarchical structure and nonlinear activation functions, excel at modeling complex nonlinear relationships, enabling them to capture intricate patterns and interactions within the data.[24] As a result, CNN can capture task-driven correlations, leading to a better understanding of the internal relationships among samples. Subsequently, a brief discussion is presented regarding the variation in accuracy relative to the size of the dataset, using a CNN. The details are illustrated in Fig. S1 (ESI†). As the sample size increases, a reduction in RMSE and an increase in R^2 are observed, indicating that larger datasets enhance the model's predictive accuracy. However, due to the relatively small dataset available for LEDs based on a new material system, transfer learning[25] (which allows models pre-trained on larger, similar datasets to be fine-tuned on smaller datasets) and data augmentation[26] (which artificially increases the diversity of training samples through various techniques) are identified as potential solutions.

Feature importance analysis

SHAP[23] is widely used to quantify the contribution of each feature to the prediction results, helping to understand the reasons behind model decisions, thereby revealing the underlying mechanisms in the data and the importance of features.[23] Through this approach, the impact of each input feature on the model output is comprehended, augmenting the interpretability and credibility of the model. Fig. 3 illustrates the interpretability analysis performed on the model utilizing the SHAP method. Fig. 3(a). displays the global importance of the top 15 features, determined by the average magnitude of SHAP values. In Fig. 3(b) and (c), we calculate the SHAP value of each feature for every prediction sample. The deviation of each point from the SHAP = 0 line intuitively represents the influence of that feature value on LOPD. Thus, the relationship between the feature value and SHAP value guides device optimization and the discovery of underlying physical mechanisms. Among the electrical characteristic parameters influencing LOPD, it is observed that the current density exerts a significantly positive impact on LOPD, indicating a direct correlation between increasing current density and higher LOPD values. Conversely, an increase in the Auger value demonstrates a negative effect on the output. Concurrently, a higher SRH lifetime value exhibits a positive influence on the output. These observations align with established physical principles.[27] Here, we focus specifically on the impact of structural characteristic parameters of LEDs devices on LOPD. As depicted in Fig. 3(c), it is evident that P1-dop (magnesium (Mg) doping concentration in the first piece of the p-type AlGaN layer) ranks first in its

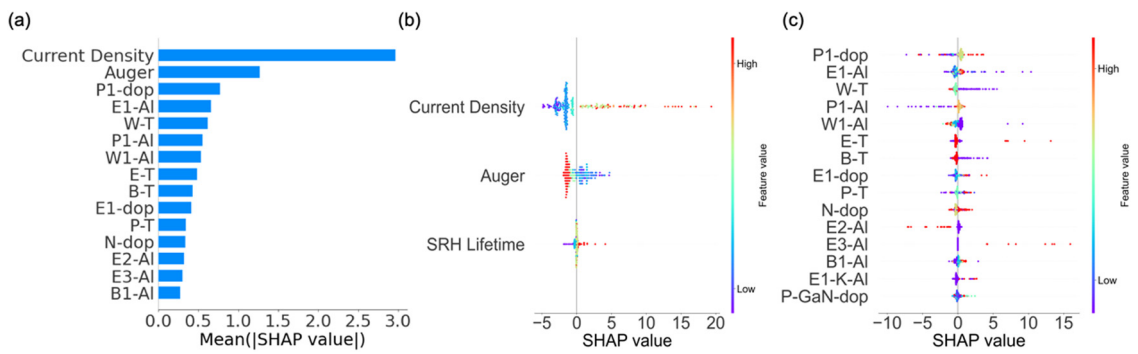

Fig. 3 Performing interpretable analysis of the model using SHAP. (a) The global importance of top 15 features based on the average SHAP value magnitude. (b) A set of scatter plots corresponding to electrical characteristic parameters. Each row in the training set is plotted based on the feature values of each data point (represented in a color scale) and their corresponding SHAP values: the vertical axis displays the sorted electrical characteristic parameters while the horizontal axis shows the SHAP values, with more positive SHAP values indicating a greater positive influence of the feature values on the model output. (c) A set of scatter plots corresponding to structural characteristic parameters.

influence on LOPD. In DUV LEDs, compared to n-type doping, p-type doping of AlGaN appears particularly challenging. With an increase in the Al content, the p-type doping efficiency of AlGaN dramatically decreases. This is primarily due to the high activation energy of Mg acceptors,[28] low solubility of Mg in AlGaN,[29,30] and severe nitrogen vacancy self-compensation.[31] Furthermore, it is also notable that E1-Al (average aluminum content in the first piece of the electron blocking layer) and W-T (total thickness of each well) rank prominently. As shown in Fig. S2 (ESI†), the experimental results indicate that E1-Al is a critical feature in AlGaN-based DUV LEDs, with its underlying mechanism exhibiting significant multidimensional coupling characteristics.[32] Conversely, W-T exhibits a clear trend in its impact on the output. Specifically, when the numerical value is relatively small, it exerts a markedly positive effect on LOPD. What is more, in feature selection for AlGaN DUV LEDs, a more complex feature modeling approach is employed, with features that significantly influence luminous performance. As shown in Fig. 3(c), features such as E2-Al and E3-Al are ranked among the top fifteen most important features. A higher value of E2-Al is found to potentially have a negative impact on LOPD, while a higher value of E3-Al may contribute positively to LOPD. These findings highlight the intricate relationships between structural characteristic parameters and LEDs performance.

ML prediction and analysis

Based on the analysis results above, the p-type AlGaN layer significantly influences the device performance of the LEDs. Building upon this observation, we design a conventional device structure. By varying the values of three parameters, namely P1-dop, P1-Al (average aluminum content in the first piece of the p-type AlGaN layer), and P-T (total thickness of the p-type AlGaN layer), we utilize our model to predict LOPD. These predictions provide insights into the impact of these three features on LOPD. The discussed LED structure is grown on a *c*-plane AlN template. Initially, a 3 μm $Al_{0.6}Ga_{0.4}N$ (Si: 5×10^{18} cm^{-3}) is grown as the electron injection layer. This layer is followed by five pairs of AlGaN/AlGaN multiple quantum wells comprising 12 nm $Al_{0.5}Ga_{0.5}N$ quantum barriers and 3 nm $Al_{0.4}Ga_{0.6}N$ quantum wells. On top of the active region is a 20-nm-thick Mg-doped (Mg: 5×10^{19} cm^{-3}) p-type $Al_{0.75}Ga_{0.25}N$ EBL and p-type $Al_xGa_{1-x}N$. Finally, a 120-nm-thick p-type GaN (Mg: 2×10^{19} cm^{-3}) contact layer completes the structure. For the p-type layer of $Al_xGa_{1-x}N$, P1-dop varies within the range of 2×10^{18} cm^{-3} to 3×10^{19} cm^{-3} with a step size of 2×10^{18} cm^{-3}, P-T ranges from 10 to 50 nm with a step size of 5 nm, while P1-Al varies within the range of 0.3 to 0.7 with a step size of 0.02.

As shown in Fig. 4(a), LOPD reaches its peak around P1-dop $\approx 1.8 \times 10^{19}$ cm^{-3}, P-T $\approx$ 45 nm, and P1-Al $\approx$ 0.48. Additionally, it is observed that compared to the P1-dop and P1-Al axes, the color variation of LOPD along the P-T axis is relatively small, indicating that the influence of the features ranked higher in importance (P1-dop and P1-Al) on LOPD outweighs that of P-T. For more clarity, the 3D-thermal contour map of the LOPD prediction with respect to P1-dop and P1-Al is extracted from Fig. 4(a). and plotted in Fig. 4(b). From Fig. 4(b), it can be observed that with the increase of P1-dop, LOPD exhibits a trend of initially increasing and then decreasing. This is attributed to the enhancement of hole concentration when increasing the p-type AlGaN doping level. However, excessive doping concentration in the p-type AlGaN layer can introduce additional impurities and defects, resulting in a decline in crystal quality. These defects act as non-radiative recombination centers, which reduce the radiative recombination efficiency of electrons and holes, ultimately leading to a decrease in light emission intensity.[31] Similarly, concerning the feature of P1-Al, a similar trend is observed. When the Al content in the p-type AlGaN layer increases, the tunneling effect of carriers is enhanced, making it easier for carriers to tunnel from the p-type AlGaN layer to the quantum well, thereby increasing the chances of radiative recombination. However, as the Al content further increases, the crystal quality of the material may deteriorate. This deterioration can lead to more defects and scattering centers, which in turn reduce the light emission intensity. For III-nitrides, p-type doping is significantly more challenging than n-type doping. In the case of GaN, the activation energy of p-type-doped Mg acceptor is approximately 160 meV, thereby resulting in a hole concentration 1 to 2 orders of magnitude lower than the electron concentration. This issue becomes much serious as the Al content in AlGaN increases.[33,34]

On the basis of the previous work, we further optimize the device structure by varying W1-Al (average aluminum content in

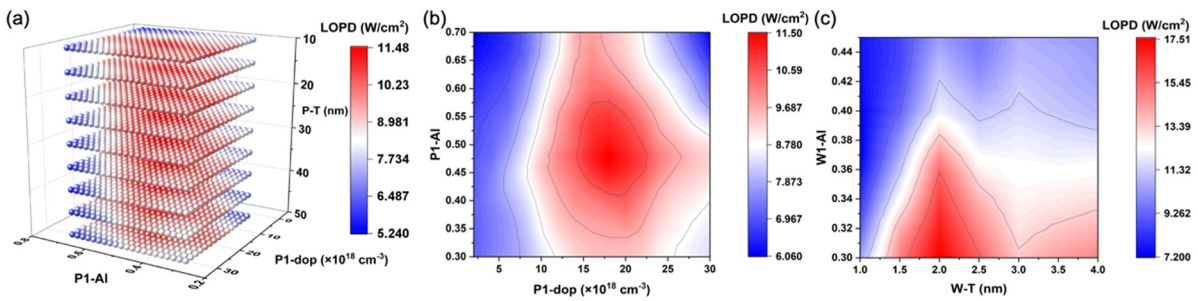

Fig. 4 Predicted LOPD with changing of different features. (a) 4D-scatter plot of LOPD with respect to P1-Al, P1-dop, and P-T. (b) 3D-thermal contour map of LOPD predictions with respect to P1-Al and P1-dop, when P-T = 45 nm. (c) 3D-thermal contour map of LOPD predictions with respect to W1-Al and W-T. Note that the predictions here are optimized on the basis of the p-type AlGaN layer.

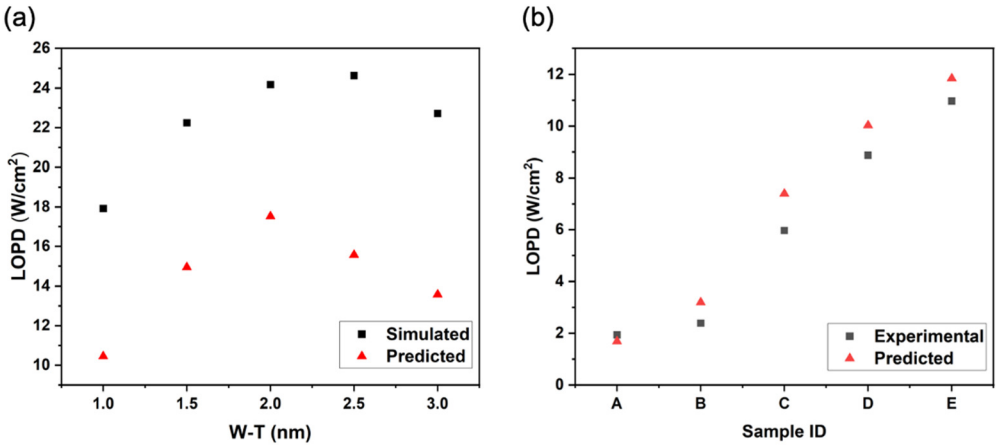

Fig. 5 Model reliability validation. (a) Comparison of CNN and APSYS prediction results. Predicted in the figure indicates the predicted result by CNN, Simulated indicates the simulated result by APSYS. (b) Comparison of CNN prediction and experimental results. Predicted in the figure indicates the predicted result by CNN, experimental indicates the experimental result from published literatures.

the first piece of the well) and W-T. The range of W1-Al is set from 0.3 to 0.45 with a step size of 0.01, ensuring it remains within the DUV wavelength range. Meanwhile, W-T ranges from 1 to 4 nm with a step size of 0.5 nm. The results are depicted in Fig. 4(c), where it can be observed that by varying these two parameters, the peak LOPD is enhanced, increasing from 11.5 W cm^{-2} to 17.51 W cm^{-2}. At this point, W-T is set to 2 nm, while W1-Al is set to 0.3. Increasing the thickness of the quantum well leads to an increase in the volume of the active region, which can accommodate more carriers and thus enhance the probability of radiative recombination.[35] As the thickness of the quantum wells increases, the separation of the electron and hole wavefunctions is enhanced, which corresponds to the quantum-confined Stark effect (QCSE). This effect can reduce the overlap of carrier wavefunctions, thereby suppressing carrier radiative recombination and resulting in decreased luminous performance.[36–38] Light emitted from the active layers can only escape through the top and bottom surfaces if it is within the escape cone.[39] The emitted photons within this cone can escape since the polarization of the emitted light is predominantly perpendicular to the crystal axis ($E \perp c$) in this region. However, for AlGaN-based DUV LEDs, as the Al content in the $Al_xGa_{1-x}N$ quantum wells increases, the proportion of the transverse magnetic (TM) wave also rises, affecting the band edge emission energy. In conventional DUV LEDs, this characteristic hinders the majority of photons produced in the active layers from escaping the cone. Thus, light extraction efficiency is extremely low for DUV LEDs.[40] Moreover, as W1-Al increases, it increases lattice mismatch and defects within the device structure, also leading to a degradation in luminous performance.[41] Therefore, it is recommended to begin with these top key parameters for initial optimization and adjustment to improve the overall performance of the DUV LEDs. Building upon this, further optimization of additional parameters is carried out, taking into account the coupling effects between different parameters.

Simulation and experimental verification

To ensure whether the model can provide reliable guidance for practical experiments, we first utilize the software APSYS to conduct simulations on the aforementioned structural configurations. In total, five structures are simulated, with W-T serving as the variable while W1-Al remains constant at 0.3. As shown in Fig. 5(a), the trends observed in the results from the APSYS simulations closely match those predicted by our model, demonstrating a similar pattern of initially increasing and then decreasing with thickness variation. As discussed in section ML prediction and analysis, increasing the thickness of the quantum well enlarges the volume of the active region, which can accommodate more carriers. However, further increasing the quantum well thickness exacerbates the QCSE, leading to reduced radiative recombination efficiency. However, it is noticed that the the predicted results in Fig. 5(a) do not perfectly align with the simulation results. This discrepancy may be attributed to variations in light extraction efficiency associated with different fabrication processes. During the data collection phase, each article employed different values for light extraction efficiency, and this variation is not accounted for during data selection.[17] To compare with experimental results, five structures from published literatures are selected (these experimental data are excluded from the training set to prevent data leakage).[12,42–45] As shown in Fig. 5(b), the predicted LOPD values closely align with the corresponding experimental results, further indicating that the model can provide guidance for experiments.

Conclusions

In this study, we introduce a ML algorithm for structural optimization of DUV LEDs. A CNN model is utilized to accurately predict the luminous performance of AlGaN-based DUV LEDs, compared with other models, including RF, XGBoost and FNN. For LOPD prediction, the CNN model achieves a R^2 of 0.9812 and a RMSE of 1.6995 W cm^{-2}. SHAP analysis quantifies the impact of each feature on LOPD, highlighting the importance of different features and revealing the key characteristics influencing the luminous performance of AlGaN-based DUV

LEDs. Following that, by integrating predictive data with existing theories, the study examines how structural characteristic parameters of AlGaN-based DUV LEDs affect LOPD. This ML approach not only deepens the understanding of DUV LEDs design principles but also provides a robust framework for guiding future experimental work and optimizing device performance. Furthermore, it holds significant potential for reducing the cost, time, and labor associated with device manufacturing, making it as a highly efficient and scalable solution for advancing DUV LEDs technology.

Author contributions

N. L.: formal analysis, investigation, software, methodology, writing – original draft; Z. L.: formal analysis, investigation, methodology, resources; Z. J.: conceptualization, software, formal analysis; Y. J.: conceptualization, resource; S. Z.: software, formal analysis; J. Y.: investigation, validation; S. J. and W. W.: investigation, methodology; Y. Y., S. L., Z. W. and J. D.: visualization, investigation; J. L. and T. T.: supervision, project administration, funding acquisition; K. H., L. L., M. C., C. L. and R. Z.: supervision, project administration, funding acquisition, writing – review & editing. All authors gave final approval for publication and agreed to be held accountable for the work performed therein.

Data availability

The authors declare that all data supporting the results reported in this study are available within the paper and the ESI.† Additional data used for the study are available from the corresponding authors upon reasonable request.

Conflicts of interest

The authors declare no competing financial interest.

Acknowledgements

This work was supported by the National Key Research and Development Program (2023YFB3611203). This work was supported by National Natural Science Foundation of China (62371407 and 62174141).

References

1 P. E. Hockberger, *Photochem. Photobiol.*, 2002, **76**, 561–579.
2 N. F. Gray, *Microbiology of Waterborne Diseases*, 2nd edn, 2014, pp. 617–630.
3 Z. Y. Xu and B. M. Sadler, *IEEE Commun. Mag.*, 2008, **46**, 67–73.
4 M. Schreiner, J. Martinez-Abaigar, J. Glaab and M. Jansen, *Opt. Photonik*, 2014, **9**, 34–37.
5 J. Chen, S. Loeb and J. H. Kim, *Environ. Sci.: Water Res. Technol.*, 2017, **3**, 188–202.
6 Y. X. Chen, J. W. Ben, F. J. Xu, J. C. Li, Y. Chen, X. J. Sun and D. B. Li, *Fundam. Res.*, 2021, **1**, 717–734.
7 T. Takano, T. Mino, J. Sakai, N. Noguchi, K. Tsubaki and H. Hirayama, *Appl. Phys. Express*, 2017, **10**, 031002.
8 H. Amano, R. Collazo, C. D. Santi, S. Einfeldt, M. Funato, J. Glaab, S. Hagedorn, A. Hirano, H. Hirayama, R. Ishii, Y. Kashima, Y. Kawakami, R. Kirste, M. Kneissl, R. Martin, F. Mehnke, M. Meneghini, A. Ougazzaden, P. J. Parbrook, S. Rajan, P. Reddy, F. Römer, J. Ruschel, B. Sarkar, F. Scholz, L. J. Schowalter, P. Shields, Z. Sitar, L. Sulmoni, T. Wang, T. Wernicke, M. Weyers, B. Witzigmann, Y.-R. Wu, T. Wunderer and Y. Zhang, *J. Phys. D: Appl. Phys.*, 2020, **53**, 503001.
9 K. B. Nam, J. Li, M. L. Nakarmi, J. Y. Lin and H. X. Jiang, *Appl. Phys. Lett.*, 2004, **84**, 5264–5266.
10 M. Kneissl, T. Y. Seong, J. Han and H. Amano, *Nat. Photonics*, 2019, **13**, 233–244.
11 L. Chen, J. J. Zheng, W. Lin, J. C. Li, K. Y. Li, P. Sun, G. Y. Guo and J. Y. Kang, *ACS Photonics*, 2017, **4**, 2197–2202.
12 Z. H. Zhang, J. Q. Kou, S. W. Huang Chen, H. Shao, J. M. Che, C. S. Chu, K. K. Tian, Y. H. Zhang, W. G. Bi and H. C. Kuo, *Photonics Res.*, 2019, **7**, B1–B6.
13 J. H. Hu, J. Zhang, Y. Zhang, H. Zhang, H. L. Long, Q. Chen, M. C. Shan, S. D. Du, J. N. Dai and C. Q. Chen, *Nanoscale Res. Lett.*, 2019, **14**, 347.
14 X. F. Ye, A. Z. Zhang, J. X. Huang, W. Y. Kang, W. Jisng, X. Li, J. Yin and J. Y. Kang, *Aggregate*, 2024, **5**, e524.
15 S. S. Zhao, J. Wang, Z. L. Guo, H. Q. Luo, L. H. Lu, Y. Y. Tian, Z. Y. Jiang, J. Zhang, M. Y. Chen, L. Li and C. Li, *J. Energy Chem.*, 2024, **94**, 441–448.
16 I. J. Choi, A. Amin, A. Katware, S. W. Kang and J. H. Lee, *ACS Photonics*, 2024, **11**, 2938–2945.
17 Z. Y. Jiang, Y. Jiang, M. Y. Chen, J. C. Li, P. G. Li, B. H. Chen, S. S. Zhao, J. Wang, S. J. Jiang, M. M. Cai, L. Li, C. Li, K. Huang, W. F. Lu, J. Y. Kang and R. Zhang, *Laser Photonics Rev.*, 2023, **17**, 2300113.
18 R. Y. Lin, Z. Y. Liu, P. Han, R. H. Lin, Y. Lu, H. C. Cao, X. Tang, C. J. Wang, V. Khandelwal, X. L. Zhang and X. H. Li, *J. Mater. Chem. C*, 2022, **10**, 17602–17610.
19 L. Breiman, *Mach. Learn.*, 2001, **45**, 5–32.
20 T. Q. Chen and C. Guestrin, Proceedings of the 22nd ACM SIGKDD International Conference on Knowledge Discovery and Data Mining, 2016, pp. 785–794.
21 W. S. Mcculloch and W. Pitts, *Bull. Math. Biophys.*, 1943, **5**, 115–133.
22 Y. Lecun and Y. Bengio, *Handbook of Brain Theory and Neural Networks*, MIT Press, Cambridge, 1995.
23 S. M. Lundberg and S. I. Lee, in *Proceedings of the 31st International Conference on Neural Information Processing Systems*, Curran Associates Inc., Red Hook, NY, USA, 2017, pp. 4768–4777.
24 K. M. He, X. Y. Zhang, S. Q. Ren and J. Sun, *IEEE Trans. Pattern Anal. Mach. Intell.*, 2015, **37**, 1904–1916.
25 D. Jha, K. Choudhary, F. Tavazza, W. K. Liao, A. Choudhary, C. Campbell and A. Agrawal, *Nat. Commun.*, 2019, **10**, 5316.

26 Y. Kim, Y. Kim, C. Yang, K. Park, G. Gu and S. Ryu, *npj Comput. Mater.*, 2021, **7**, 140.
27 J. Y. Chang, Y. H. Shih, M. F. Huang, F. M. Chen and Y. K. Kuo, *Phys. Status Solidi A*, 2018, **215**, 1800271.
28 K. B. Nam, M. L. Nakarmi, J. Li, J. Y. Lin and H. X. Jiang, *Appl. Phys. Lett.*, 2003, **83**, 878–880.
29 T. Kinoshita, T. Obata, H. Yanagi and S. I. Inoue, *Appl. Phys. Lett.*, 2013, **102**, 012105.
30 J. Wang, W. T. Cai, W. F. Lu, S. Lu, E. Kano, V. C. Agulto, B. Sarkar, H. Watanabe, N. Ikarashi, T. Iwamoto, M. Nakajima, Y. Honda and H. Amono, *Nature*, 2024, **631**, 67–72.
31 F. Shahedipour and B. W. Wessels, *Appl. Phys. Lett.*, 2000, **76**, 3011–3013.
32 Y. K. Kuo, F. M. Chen, J. Y. Chang, M. F. Huang, B. T. Liou and Y. H. Shih, *IEEE J. Quantum Electron.*, 2020, **56**, 1–6.
33 C. Stampfl and C. G. Van de Walle, *Phys. Rev. B: Condens. Matter Mater. Phys.*, 2002, **65**, 155212.
34 J. C. Li, N. Gao, D. J. Cai, W. Lin, K. Huang, S. P. Li and J. Y. Kang, *Light: Sci. Appl.*, 2021, **10**, 129.
35 T. S. X. Tan, J. C. Zhang, T. Egawa, G. Chen, X. D. Luo, L. Sun and Y. H. Zhu, *Nanoscale Res. Lett.*, 2018, **13**, 334.
36 N. Grandjean, B. Damilano, S. Dalmasso, M. Leroux, M. Laugt and J. Massies, *J. Appl. Phys.*, 1999, **86**, 3714–3720.
37 T. Kolbe, T. Sembdner, A. Knauer, V. Kueller, H. Rodrihuez, S. Einfeldt, P. Vogt, M. Weyers and M. Kneissl, *Phys. Status Solidi A*, 2010, **207**, 2198–2200.
38 X. Liu, Z. X. lv, Z. F. Liao, Y. C. Sun, Z. Q. Zhang, K. Sun, Q. X. Zhou, B. Tang, H. S. Geng, S. L. Qi and S. J. Zhou, *Microsyst. Nanoeng.*, 2024, **10**, 110.
39 T. N. Oder, K. H. Kim, J. Y. Lin and H. X. Jiang, *Appl. Phys. Lett.*, 2004, **84**, 466–468.
40 N. Gao, K. Huang, J. Li, S. Li, X. Yang and J. Kang, *Sci. Rep.*, 2012, **2**, 816.
41 H. Hirayama, N. Maeda, S. Fujikawa, S. Toyoda and N. Kamata, *Jpn. J. Appl. Phys.*, 2014, **53**, 100209.
42 J. C. Yan, J. X. Wang, Y. Zhang, P. P. Cong, L. L. Sun, Y. D. Tian, C. Zhao and J. M. Li, *J. Cryst. Growth*, 2015, **414**, 254–257.
43 Z. H. Zhang, S. W. Huang Chen, Y. H. Zhang, L. P. Li, S. W. Wang, K. K. Tian, C. S. Chu, M. Q. Fang, H. C. Kuo and W. G. Bi, *ACS Photonics*, 2017, **4**, 1846–1850.
44 A. Fujioka, T. Misaki, T. Murayama, Y. Narukawa and T. Mukai, *Appl. Phys. Express*, 2010, **3**, 041001.
45 C. S. Chu, K. K. Tian, J. M. Che, H. Shao, J. Q. Kou, Y. H. Zhang, M. Y. Wang, Y. H. Zhu and Z. H. Zhang, *Opt. Express*, 2019, **27**, A620–A628.

